Control of the size, shape and composition of highly uniform, non-agglomerated, sub-micrometer β-tricalcium phosphate and dicalcium phosphate platelets

CrossMark

Laetitia Galea [a,b], Marc Bohner [a,*], Juerg Thuering [a,c], Nicola Doebelin [a], Christos G. Aneziris [b], Thomas Graule [b,d]

[a] RMS Foundation, Bischmattstrasse 12, CH-2544 Bettlach, Switzerland
[b] Technical University Bergakademie Freiberg, Institute for Ceramic, Glass and Construction Materials, Agricolastraße 17, 09596 Freiberg, Germany
[c] ETH Zürich, Department of Materials, Laboratory of Multifunctional Materials, Wolfgang-Pauli-Strasse 10, 8093 Zürich, Switzerland
[d] EMPA, Swiss Federal Laboratories for Materials Science and Technology, Laboratory for High Performance Ceramics, Ueberlandstrasse 129, 8600 Dübendorf, Switzerland

ARTICLE INFO

ABSTRACT

Calcium phosphates (CaPs) are widely used as bone graft substitutes but are inherently brittle, hence restricting their use to mechanically protected environments. Combining them with a tough polymer matrix could potentially lead to a composite with load-bearing properties. However, the highest mechanical properties can only be achieved if the CaP particles possess very precise features: they should be uniform in size and shape, non-agglomerated, elongated and thin. The aim of the present study therefore was to assess a novel method to produce such particles. This involved the precipitation of CaP particles in ethylene glycol at moderate temperatures (90–170 °C) and the variation of different reaction parameters (temperature, concentration, pH, etc) to study their influence on particle composition, size, shape and dispersion was studied. As a result, two main CaP phases were obtained as well-dispersed and highly uniform platelets in the form of: (i) β-tricalcium phosphate (β-TCP) hexagonal prisms and (ii) monetite (DCP) flat parallelepipeds. The size dispersion was the narrowest for β-TCP (standard deviation/mean < 5%) whereas the aspect ratio was the highest for DCP (up to 25). In both cases, the thickness of the platelets was below 300 nm which should be ideal for the synthesis of strong CaP-based composites.

© 2013 Elsevier Ltd. All rights reserved.

1. Introduction

In the past decades synthetic bone graft substitutes have become a viable alternative to bone auto and allografts which, although still being considered as the gold standard for bone void filling by many surgeons, have some important drawbacks: high costs and risks of disease transmission in the case of allografts [1], and limited availability, additional pain and an increased risk of side-effects for autografts [2,3].

Calcium phosphates (CaP) ceramics are widely used as a synthetic alternative due to their chemical similarity to the mineral part of bone [4,5]. There is a broad range of CaP materials used for bone substitution. The most common ones are sintered CaP, such as

hydroxyapatite (HA, $Ca_5(PO_4)_3OH$), β-tricalcium phosphate (β-TCP, $Ca_3(PO_4)_2$) and their mixtures called biphasic calcium phosphates (BCP). β-TCP is of particular interest as it is generally considered to be an excellent bone substitute, not only presenting a high osteo-conductivity but also, and contrary to sintered HA [6], a cell-mediated resorption [5,7]. Calcium and phosphate ions released during the resorption can be used to mineralize new bone in the bone remodelling process [8]. Also other non-sintered CaP phases such as brushite (DCPD, $CaHPO_4 \cdot H_2O$) and monetite (DCP, $CaHPO_4$) have recently raised the interest of researchers due to their good biocompatibility and fast osteotransduction [9–11]. Their degradation pathway is similar to that of β-TCP but has been less studied as for β-TCP due to their younger history as implant materials.

A major drawback of synthetic CaP bone substitutes is their brittleness [12], which prevents their use in load-bearing applications [1]. To overcome this problem, the current trend is to combine CaP particles with a degradable polymer [1,13]: the ceramic

* Corresponding author. Tel.: +41 32 6441413.
E-mail address: marc.bohner@rms-foundation.ch (M. Bohner).

particles provide strength and stiffness to the composites, while the polymer phase brings toughness [14]. However, to optimize this mechanical reinforcement, the ceramic particles must have very precise features: (i) they must be non-agglomerated to prevent voids [15] and crack propagation by weak and brittle particle interactions [16]; in addition agglomerates locally impair alignment of the particles. (ii) They must have one or preferably two dimensional geometries (fibers or platelets) to eventually provide a unidirectional or preferentially planar reinforcement of the composite [17,18]. (iii) They must have a high aspect ratio to provide a large contact area and optimal load transfer between polymer matrix and ceramic particles [19]. (iv) They must be thinner than a critical size under which ceramic particles reach their maximum mechanical properties [20]. (v) They must be uniform in size (=monodisperse) to achieve homogeneous properties. A regular shape and size also helps to achieve high packing density and consequently high ceramic fractions, as observed in tough natural materials like nacre [21].

So far, such a good control of CaP particle features has not been achieved with current manufacturing processes. CaP powders are usually obtained by either high temperature processes (solid-state reaction, thermal conversion) or wet chemical routes (precipitation, hydrolysis). When produced by sintering or by solid-state reaction at high temperature (α-TCP, β-TCP, HA), the particles are agglomerated, have a low aspect ratio and broad size distributions [22]. Contrarily, when synthesized by precipitation, higher aspect ratios can be achieved but still a high degree of agglomeration and large size and geometry variations are observed [23–26]. Less agglomeration is generally reported for hydrothermally produced CaP particles. Needles or whiskers are commonly observed but the particle size distribution remains quite broad [27–32]. For example, Zhang and Darvell [27,28] obtained needles with a size dispersion estimated at 0.2–0.3 (standard deviation/mean). Zhang et al. [32] obtained HA platelets with a length between 25 and 160 nm, i.e. a size dispersion (=standard deviation/mean) of about 0.5. Monodispersity is usually defined as <0.10 [33].

Recently Tao et al. [34,35] proposed to synthesize single hexagonal β-TCP crystals by precipitation in ethylene glycol. This study describes the precipitation of nearly uniform, non-agglomerated, sub-micrometer CaP particles. The loose, homogeneous and well-defined particles obtained by Tao et al. [34,35] would allow a high packing density in a composite material, but would not be sufficient to efficiently reinforce a polymer matrix because of their low aspect ratio (3–4). In order to optimize the mechanical properties of the composite, it is necessary to increase the length and aspect ratio of the crystals. Therefore the aim of the present study was to extend Tao's work in order to synthesize CaP particles of controlled thickness, aspect ratio and composition, a low degree of agglomeration and high productivity. A more specific aim was to obtain CaP particles with considerably higher aspect ratios (typically >20) as those observed by Tao et al. (3–4), irrespective of the CaP crystalline phase. For that purpose, various parameters were

systematically modified and the yielded crystals were characterized extensively, while particular attention was paid to the reproducibility of the experiments.

2. Materials and methods

2.1. Precipitation method

The precipitation reaction used here was inspired by Tao et al. [34]. Briefly, an ethylene glycol ($C_2H_6O_2$, Reag.Ph.Eur., art. no85512.360, VWR, Nyon, Switzerland) solution containing phosphate ions ($Na_2HPO_4 \cdot 2H_2O$, purum p.a., art. no71645, Fluka, Buchs, Switzerland) was poured into a pre-heated ethylene glycol solution that contained calcium ions ($CaCl_2 \cdot 2H_2O$, Reag.Ph.Eur., art. no1.02382, MERCK, Darmstadt, Germany). After 1.5 h reaction, the solution was cooled down and centrifuged at 4000 rpm for 30 min to separate the solid phase from the filtrate. The precipitate was then washed by mixing and centrifugation cycles in alternating demineralised water and ethanol (C_2H_6O, absolute 99.8%, art. noG003, Grogg, Switzerland). After washing, the precipitate was dispersed again in ethanol and small amounts of this suspension were used for scanning electron microscopy (SEM), X-ray diffraction (XRD) and particle size measurements. The remains were dried at 30 °C under vacuum (vacuum drying oven from Binder, Tuttlingen, Germany) for 24 h. A standard experiment was defined as having a total volume of 70 mL, a titration rate of around 600 mL/min (=highest rate that can be achieved by manually pouring the phosphate solution into the calcium solution), a reaction temperature of 150 °C, a total precursors' concentration (sum of phosphate and calcium ions) of 16 mM, a Ca/P molar ratio of 1.5 and a pH of the phosphate solution of 9.5 (adjusted at 95 °C with NaOH, puriss. p.a., art. no 71690, Fluka, Buchs, Switzerland) (Table 1).

2.2. Reaction parameters

Several parameters were modified to achieve various aims (Table 1): (i) increase the productivity, by increasing the reagent volume (from 70 to 500 mL) or the total precursors concentration (from 1.6 to 64 mM) (ii) ease the production procedure by increasing the addition rate of the phosphate precursor (from 0.5 to 800 mL/min), or by reducing the production temperature below 100 °C to allow the replacement of an oil bath with a water bath, save energy and avoid long heating times, or (iii) influence the composition, size and shape of the precipitated particles by varying the solution's pH (from 4 to 10), the precursors concentration (from 1.6 to 64 mM) or the reaction temperature (from 90 to 170 °C). As the reaction rate was expected to decrease with a decrease of temperature, the reaction time was increased from 1.5 h to 24 h.

2.3. Characterization

Various characterization methods were applied to the particles. The size and morphology of the precipitate were analysed by scanning electron microscopy (SEM). Rietveld refinement of X-ray diffraction (XRD) measurements was used to quantify the relative amounts of crystalline phases. Finally, the particle size distribution (PSD) was measured by laser diffraction.

For SEM, a drop of the diluted ethanol suspension was spread on a SEM aluminium sample holder. After complete evaporation of the solvent, the samples were coated with a 10 nm thick platinum layer (sputter time 60 s at 40 mA) and observed with an EVO MA25 microscope (Zeiss, Germany) using a voltage of 20 kV and a working distance of 7–8 mm. The particle size was assessed by image analysis (Image Access 11 Premium, Imagic Bildverarbeitung AG, Glattbrugg, Switzerland) of SEM pictures at 10,000 fold enlargement. The dimensions of at least 20 particles were used to calculate the mean diameter, length and width. As most particles were lying flat, only a minimum of 6 measurements was used to determine the particle thickness. The diameter, d, of hexagonal prisms was defined as the diameter of the inscribed circle (Fig. 1, left); for parallelepiped particles, the length, l, and width, w, were measured as the length and width of the circumscribed rectangle (Fig. 1, right). The aspect ratio, s, was defined as the diameter or the length divided by the

Table 1
Description of the experiments performed in this study to assess the effects of reaction volume, titration rate, reaction temperature, precursors' concentration and pH. The parameters that were varied in each sub-study are marked in bold. The standard experiment is the reference that was used for comparison in each sub-study.

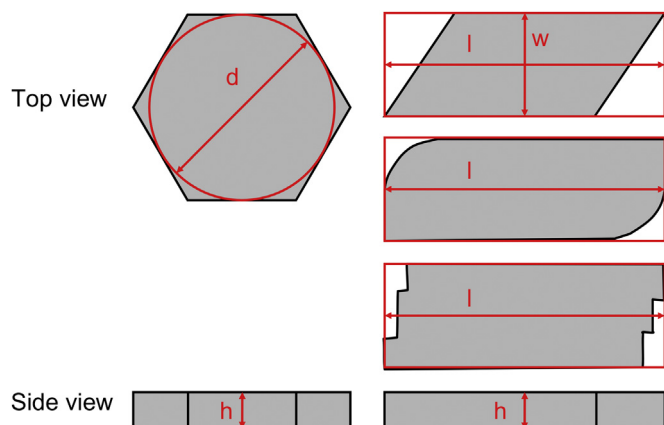|		Volume [mL]	Precursors concentration [mM]	Titration rate [mL/min]	Reaction temperature [°C]	pH of PO_4^{3-} solution	n
Standard experiment		70	16	≈600	150	9.5	5
Study of the effect of...	... volume	**70, 500**	16	≈600	150	9.5	7
	... precursors concentration	**500**	**1.6, 4, 8, 16, 32, 64**	≈800	150	9.5	1 (2)
	... titration rate	**70, 500**	16	**0.5, 20, ≈600–800**	150	9.5	2
	... reaction temperature	70	16	≈600	**90, 110, 130, 150, 170**	9.5	5 (3 at 170 °C)
	... pH	70	16	≈600	**90, 150**	**4, 7, 7.5, 8, 9.5, 10**	1 (2)

Fig. 1. Description of the measurement methods used to determine the dimensions of the hexagonal β-TCP platelets (left) and the parallelepiped DCP platelets (right). The aspect ratio is calculated as $s = d/h$ or $s = l/h$.

thickness. The ratio between the standard deviation and the mean of the longest dimension (diameter or length) was used to estimate the size dispersion.

For X-ray diffraction measurements (XRD), a concentrated ethanol suspension was dried on a glass plate, scratched off and spread on a silicon single crystal sample holder to minimize preferred orientation. XRD data were collected in reflective geometry on an X-Pert diffractometer (X'Pert Pro MPD, Panalytical, Almelo, The Netherlands). Ni-filtered CuK$_\alpha$ radiation, a step size of 0.016° and a measuring angle from 4.01° to 59.99° 2θ were used for all XRD characterizations. Semi-quantitative phase analysis was done by Rietveld refinement and the FullProf.2k software (Version 5.00) [36] using a previously determined instrument resolution function. Crystalline models for β-tricalcium phosphate (β-TCP), monetite (DCP) and chloroapatite (Cl-HA) were taken from Dickens et al. [37], Dickens et al. [38] and Sudarsanan and Young [39], respectively.

Particle size distribution (PSD) was measured with a laser diffraction particle size analyser (LS 13 320, Beckman–Coulter, Krefeld, Germany). The concentrated ethanol suspension of platelets was added drop by drop into the reservoir of the device filled with ethanol until an adequate concentration was reached. Sonication was applied for 30 s before each measurement with a sonication control unit (Beckman–Coulter, Krefeld, Germany).

2.4. Statistical analysis of results

Dimension values are given as mean ± one standard deviation. The significance of differences was evaluated by Student t-test or by ANOVA and was set at a maximum error risk of 5%.

3. Results

3.1. Reproducibility of standard experiments

One of the aims of this study was to test the reproducibility of the synthesis. For that purpose, a synthesis in "standard" conditions was performed 5 times. The standard experiment (Table 1) led to hexagonal platelets with average diameter and thickness of 853 ± 73 nm and 164 ± 11 nm, respectively (Fig. 2). As a result, the size dispersion was 0.09 and the average aspect ratio was 5.5 ± 0.7. However, it is important to mention that the size dispersion in each batch was lower than 0.05. Significant but small differences were not only seen in the mean size but also in the appearance of the platelets: variations of porosity and surface roughness were observed between batches (Fig. 2). According to laser diffraction, most of the particles were non-agglomerated, but the presence of a few 1.3 μm large particles was detected (Fig. 3). The median particle size (D_{50}) in number was 0.33 μm, i.e. much smaller than the diameter measured on SEM images. This discrepancy might be explained by artefacts in laser diffraction measurements due to the non-spherical shape of the particles, whereas the model is based on spherical particles. Hence the obtained value is an equivalent diameter, not the absolute diameter. Indeed, laser diffraction is

known to have problems estimating the size of particles with large aspect ratios, because the diameter depends on the particle orientation. However, this does not impair comparison between experiments and identification of agglomerates. The crystalline phase composition obtained by Rietveld refinement of XRD measurements was mainly β-TCP with traces (<1%) of chloroapatite (Fig. 4). However, the fit was difficult due to a preferential orientation of the β-TCP platelets along the c-axis (001 direction), as well as insufficient sample area and thickness on account of limited availability of material.

After drying, 20–30 mg of β-TCP platelets were obtained, corresponding to about 30–40% of the total amount of calcium and phosphate ions initially present in the solution.

3.2. Increase of the reagent volume to increase the productivity

A second aim of this study was to increase the productivity. One possibility to reach this goal was to increase the batch size. Fortunately, the change of reaction volume from 70 to 500 mL did not have a significant effect on the output morphology (Fig. 5), however the production in 500 mL-batches better preserved the samples and reduced their porosity. The amount of obtained platelets was between 150 and 200 mg, which is a similar productivity than with smaller volumes, i.e. 30–40% of the total amount of calcium and phosphate ions initially present in the solution.

3.3. Increase of the precursors concentration to increase the productivity and modify the particles

A second way to increase the productivity was to increase the precursors' concentration. However, since this parameter might also affect the particle appearance (geometry, size), a large range of concentrations was tested, from 10 to 400% of the standard concentration (16 mM). At 1.6 mM, hollow regular octahedron particles were obtained (Fig. 6a). At 4 mM, the obtained particles had a similar shape and were still hollow but larger (Fig. 6b). The size further increased by rising the precursors' concentration, but from 8 mM the particles became hexagonal prisms and were not hollow anymore, but porous (Fig. 6c and d). From 32 mM onwards, larger (>1 μm) parallelepiped particles appeared (Fig. 6e) and prevailed at 64 mM (Fig. 6f). Furthermore fine particles covering the surface of the prisms could also be detected at 64 mM.

The hexagonal prisms diameter enlarged with increasing precursors' concentration while the thickness tended to decrease (Fig. 7). In consequence, the aspect ratio increased from 1 to 10 (Fig. 7). Contrarily, a change in concentration did not affect the size of the parallelepiped particles that appeared at 32 and 64 mM. These particles were 3.3 ± 0.9 μm long, 1.3 ± 0.4 μm wide and 0.23 ± 0.05 μm thick, leading to an aspect ratio of 14 ± 5 and a size dispersion of 0.2.

The crystalline phase composition measured by Rietveld refinement of XRD results varied with the precursors concentration. Up to 16 mM, the samples solely consisted of β-TCP. At a concentration of 32 mM, β-TCP was mixed with 15 wt% DCP and 45 wt% chloroapatite and at 64 mM DCP was mixed with 33 wt% chloroapatite and 1 wt% β-TCP (Fig. 8).

3.4. Increase of titration rate to simplify the process

In the aim to simplify the production process, the titration rate was increased to a maximum, i.e. the phosphate solution was added into the calcium solution at once, but not without beforehand studying the effect of this parameter on the size and degree of agglomeration of the particles. In addition, variations of addition rate were investigated at two different volumes, 70 and 500 mL,
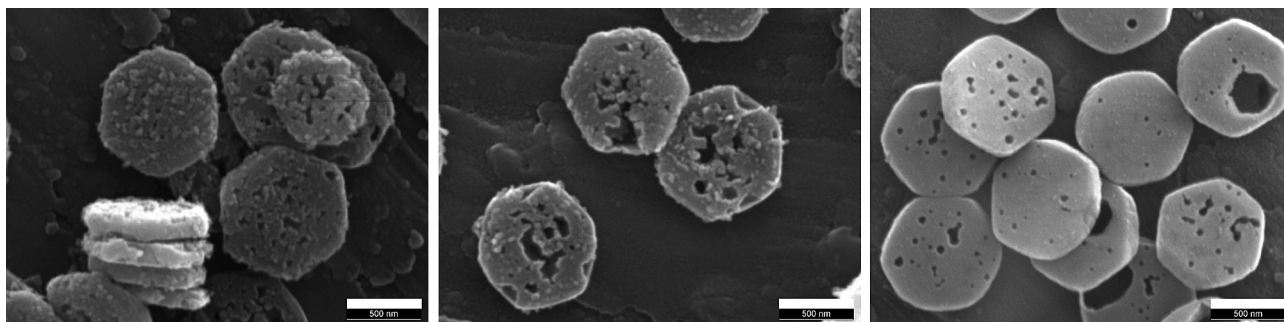
Fig. 2. Three representative batches of hexagonal platelets obtained with the standard conditions. Scale bar is 500 nm.

although the addition rate was not scaled with the volume. Hence, the titration rates are not directly comparable, since adding a solution at the same speed in a large volume increases slower the concentration than in a small volume. In consequence, for comparison, the titration rates were reported to the volume and expressed in [min⁻¹]. The lowest titration rate of 0.5 mL/min in a large volume led to agglomerated, thick and round particles (Fig. 9a); at all higher titration rates, hexagonal platelets were observed. The agglomeration decreased and the particle size and aspect ratio increased with increasing titration rate (Fig. 9b–e) until no more changes were observed at the highest titration rate between both volumes (Fig. 9c and f). Displaying the size dispersion over the titration rate relative to the total volume showed a negative tendency (Fig. 10a), i.e. the faster the addition rate, the narrower the size dispersion.

Without consideration of titration rate, the volume affected the particles appearance: when synthesized in a smaller volume, the platelets tended to be porous (Fig. 9b–c), while their surfaces were denser and smoother with a larger volume (Fig. 9e–f).

PSD measurements by laser diffraction confirmed the broadening of PSD (Fig. 10b) and the reduction of the median particle size with decrease of addition rate (results not shown). Importantly, after dispersion in ethanol and ultrasonication no agglomerates were measured.

3.5. Influence of temperature on the particles

Another way to ease the platelets synthesis is to decrease the reaction temperature. This would for instance avoid using an oil bath, save energy and reduce heating times. But the reaction temperature might affect the particles. Hence, the effect of a
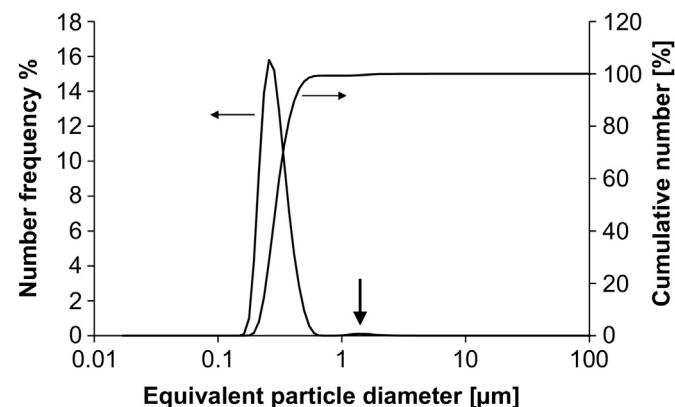
temperature change from 90 up to 170 °C was investigated. At 90 °C (Fig. 11a), the samples mostly consisted of large parallelepiped platelets with blunt edges and a sheet structure. Some small circular to hexagonal platelets were also observed. Increasing the temperature decreased the relative amount of the parallelepiped particles while the shape of both types of particles became better defined, i.e. less round and more hexagonal in the case of the small ones and the large ones developed towards a rectangular and less sheet-like shape (Fig. 11). No more parallelepipeds were observed at 150 and 170 °C. Quantitatively, the length and width of the parallelepiped platelets were significantly smaller at 130 °C than at 90 and 110 °C (Fig. 12a). Since their thickness did not vary significantly, the aspect ratio of the platelets significantly decreased from 12 ± 3 to 9 ± 3 (Fig. 12a). The size dispersion in length and width also significantly decreased with the temperature from 0.30 at 90 °C to 0.14 at 130 °C. Similar observations were made with hexagonal platelets. The diameter of the hexagonal prisms (Fig. 12b) increased significantly from 600 to 800 nm between 90 and 110 °C and was stable between 110 and 150 °C. It then decreased to 600 nm at 170 °C, though this change was not significant ($p = 0.14$). The thickness (Fig. 12b) continuously increased with the temperature between 90 and 150 °C, from 120 to 180 nm and the decrease observed at 170 °C was not significant. However, the aspect ratio (Fig. 12b) did not vary significantly between 90 and 170 °C. The size dispersion per batch of the hexagonal platelets was narrow for all temperatures and was the lowest at 130 and 150 °C (0.03–0.10 for single batches, 0.11–0.20 across multiple batches, $n = 5$).

According to Rietveld refinement of XRD data, most of the precipitates produced at 90 °C consisted of monetite (DCP) with about one-third of β-TCP and a few percent of chloroapatite (Cl-
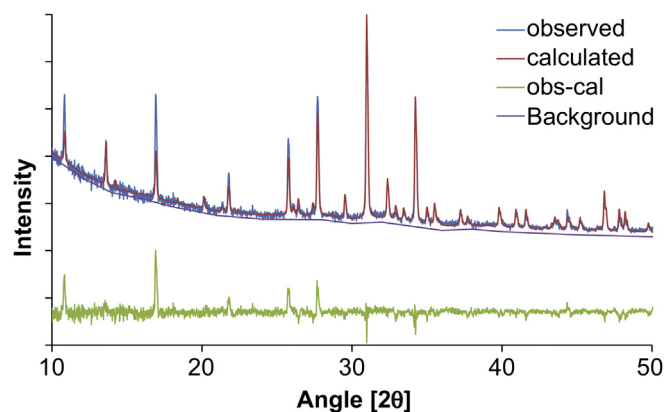

Fig. 3. Particle size distribution obtained by laser diffraction in volume percent. The arrow shows the small peak at 1.3 μm.

Fig. 4. Representative XRD of a standard experiment. The diagram corresponds to β-TCP with traces of chloroapatite. The differences (green line) between observed values (blue line) and the calculated model (red line) are due to a high crystalline orientation. (For interpretation of the references to colour in this figure legend, the reader is referred to the web version of this article.)
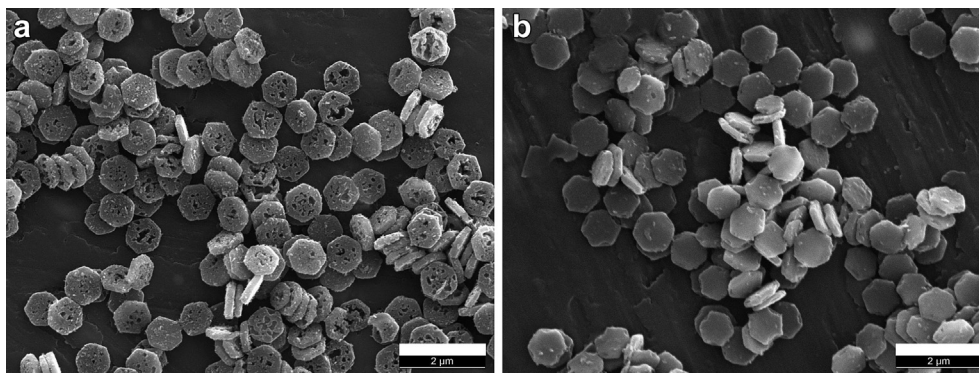
Fig. 5. Representative SEM images of batches with a) small volume (70 mL); b) large volume (500 mL). Scale bar is 2 µm.

HA). The amounts of DCP and Cl-HA decreased with increasing temperature and were negligible at 150 and 170 °C (Fig. 13).

The precursors' concentration and reaction temperature were investigated in order to increase the productivity and ease the production, respectively. These parameters were seen to affect the particles size, shape and composition. In both investigations, beside β-TCP hexagonal particles, monetite particles appeared which are usually more stable at lower pH values than β-TCP. Possibly, variations of pH might as well affect the particles shape, size and composition.
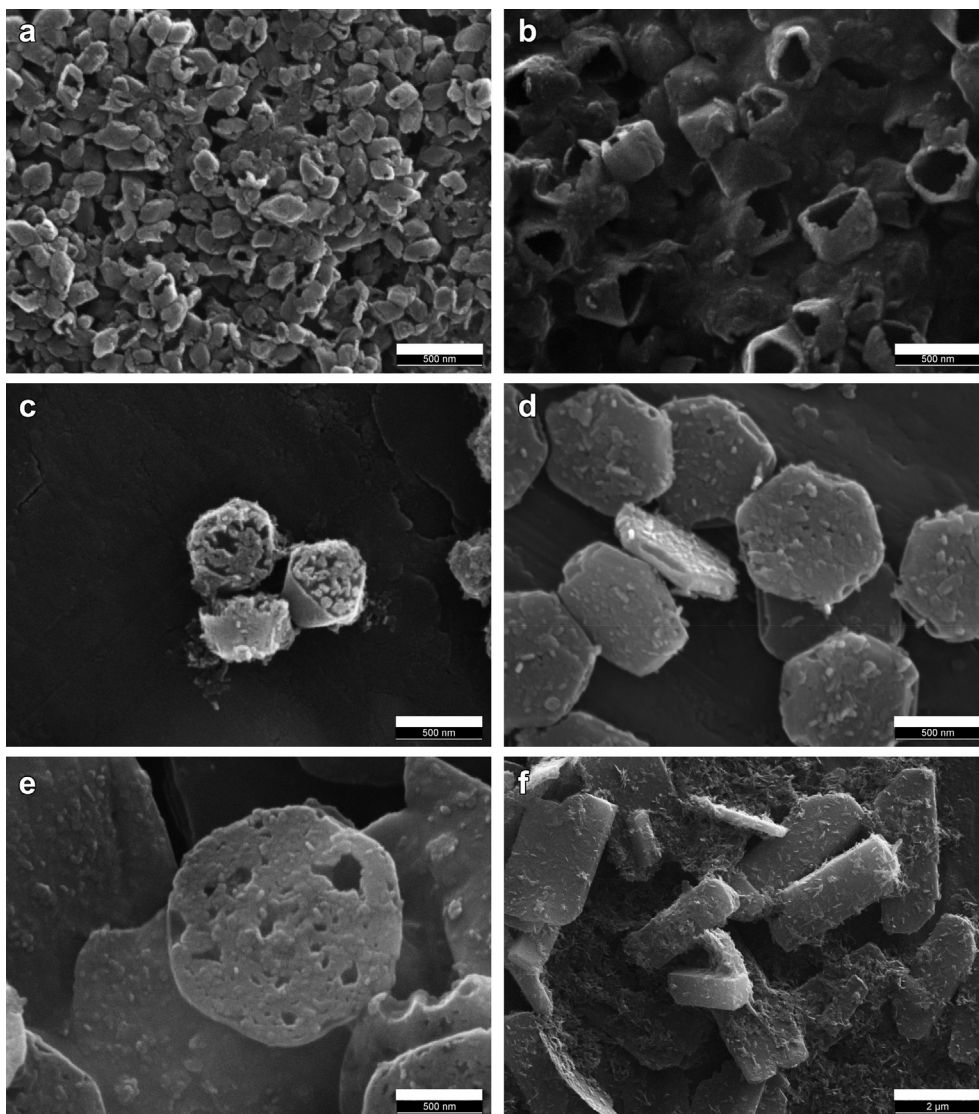

Fig. 6. Representative SEM images at different precursors concentration: a) 1.6 mᴍ; b) 4 mᴍ; c) 8 mᴍ; d) 16 mᴍ; e) 32 mᴍ; f) 64 mᴍ. Scale bar is 500 nm for a–e and 2 µm for f.
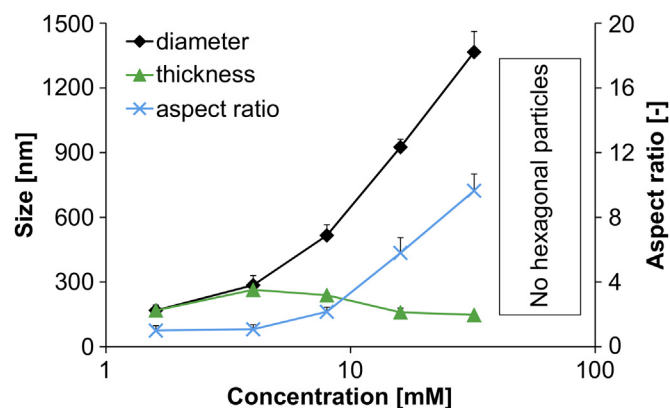
Fig. 7. Effect of the precursors concentrations on the dimensions of the hexagonal platelets: diameter (diamonds, left axis), thickness (triangles, left axis) and aspect ratio (cross, right axis).

3.6. Effect of the pH value on the particles

The effect of the pH was investigated from pH 4 to pH 10 at temperatures of 90 and 150 °C. The first difference from standard conditions was the appearance of a gel-like substance in the centrifugation tubes at the highest pH values (pH 9.5 and 10 at 90 °C and pH 10 at 150 °C), which was not observed at pH 9.5 and 150 °C. SEM observations revealed the formation of star-like particles at 90 °C and pH 4 (Fig. 14a). At 90 °C, pH 7 elongated plate-like particles were formed. These particles tended to be thicker with better defined edges when further increasing the pH (Fig. 14b and c). From pH 9.5 onwards, hexagonal platelets and a continuous phase started to appear (Fig. 14d) and remained the only phase detected at pH 10 (Fig. 14e). A similar behaviour was observed at a temperature of 150 °C. Specifically, parallelepiped platelets were observed at pH 4 and pH 7 (Fig. 14f–g). At pH 8, hexagonal platelets already appeared (Fig. 14h–j) and prevailed at pH 9.5 and pH 10. At pH 10, the continuous phase was noticed, as observed at 90 °C.

The size of the different types of particles was measured on the SEM images. The star-like particles obtained at 90 °C and pH 4 had a diameter of 2.8 ± 0.7 μm. The size of the parallelepiped particles obtained at 90 °C varied significantly as a function of pH (Fig. 15a). They were significantly longer and thinner at pH 7 than at pH 8 and pH 9.5 although the width and the size dispersion remained similar. Hence, the aspect ratio reached 23 ± 4 at pH 7, but decreased to 16 ± 4 at pH 8 and pH 9.5. Contrarily, the size of the parallelepiped particles obtained at 150 °C did not vary significantly with the change of pH, except for a 20% decrease of width between pH 7 and
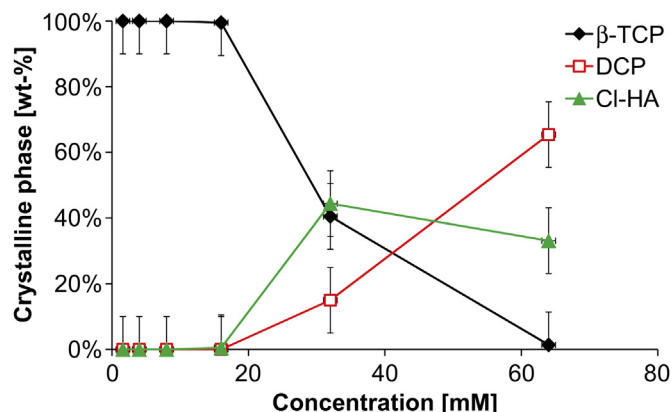

Fig. 8. Effect of the precursors concentrations on the crystalline phase.

pH 8 (Fig. 15c). Turning to the hexagonal platelets, no variation of size was observed at 90 °C (Fig. 15b). However, at 150 °C the hexagonal prisms shrunk with a pH increase (Fig. 15d). At pH 8, all platelets laid flat, so their thickness could not be measured. Hence, a comparison of the aspect ratio was not feasible. However, the platelets seemed very thin, possibly thinner than at higher pH values. Consequently, the aspect ratio was likely higher than 10.

XRD measurements and Rietveld refinement revealed that at 90 °C, up to a pH of 8, the samples consisted of pure monetite. An increase of the pH led to a mix of monetite and β-TCP and finally at pH 10 to a mix of β-TCP (77 wt%) and chloroapatite (23 wt%) (Fig. 16). The larger diffraction peaks obtained with this sample and the broad and high background indicated the presence of an amorphous phase (Fig. 17), probably the continuous phase observed in SEM. Rietveld refinement indicated a strong preferential orientation of both types of crystals, explaining the observed difference in intensity (Fig. 17). The same phase change from monetite to β-TCP was observed at 150 °C, but slightly shifted towards lower pH values (Fig. 16). At high pH values, an amorphous phase also appeared, but without occurrence of chloroapatite.

4. Discussion

The aim of this study was to produce reproducible CaP platelets of controlled thickness, aspect ratio and composition, a low degree of agglomeration and high productivity. For this purpose, $CaCl_2$ and Na_2HPO_4 salts were dissolved in ethylene glycol and these solutions were mixed and aged under controlled conditions. The effects of several parameters were investigated: pH, temperature, titration rate and concentration of precursors. The particles composition and dimensions were measured.

4.1. Reproducibility

Before investigating the effect of several parameters on the yielded particles, it was important to verify the reproducibility of the experiment. This was done by replicating 5 times the standard experiment (Table 1), which yielded hexagonal β-TCP platelets (prisms).

A high reproducibility between replicas was found (Table 2). Some size variations were observed from batch to batch, but these differences remained small (size dispersion < 10%). When looking at the literature, the particles produced here were slightly larger and thinner (diameter = 853 ± 73 nm, thickness = 164 ± 11 nm, Fig. 2) than those obtained by Tao et al. (diameter = 750–800 nm, thickness = 200–250 nm, [34]), but differences were marginal. Besides the variations of size, differences of surface appearance of the β-TCP crystals were noticed, particularly at different batch volumes: in large batches, the platelets were very smooth (Fig. 5b), whereas platelets produced in small volumes were rough or even porous (Figs. 2 and 5a). The pores and roughness were similar to the dissolution patterns observed by Tao et al. [34]. This suggests that the β-TCP platelets were dissolved during washing. In fact, the differences observed from batch to batch and in different conditions can be easily explained by the fact that the washing conditions were not the same for all samples. Indeed, some batches could be cleaned directly after precipitation, while others had to be stored for a while in solution (water or ethanol) before centrifugation due to lab use constraints. Moreover, the washing procedure was not the same for large and small batches. Specifically, the platelets produced in large volumes were 3 times more concentrated during washing.

Despite these variations, the reproducibility of the synthesis method can be considered to be excellent, even if different synthesis conditions are used (Table 2), not only in terms of particle size but also in terms of chemistry.
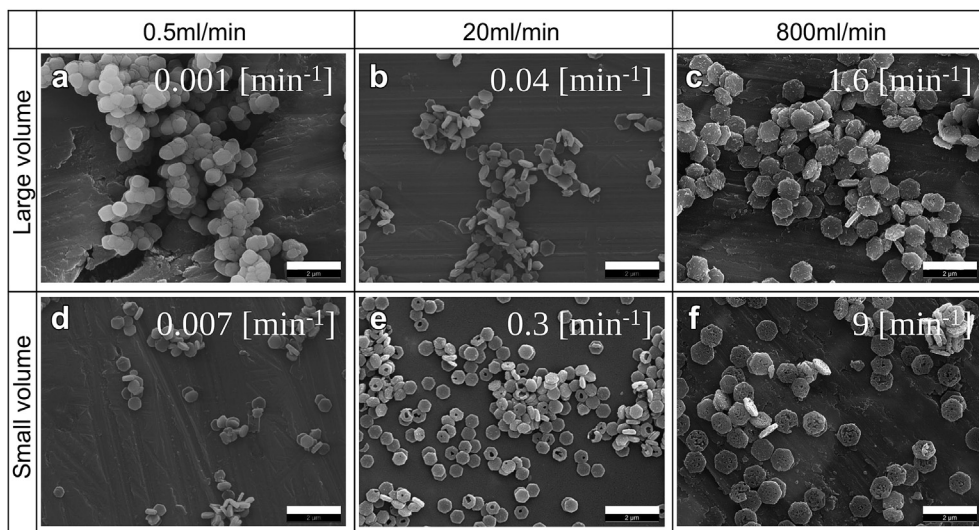
Fig. 9. SEM images of precipitates obtained in a)–c) large volume, d)–f) small volume, with a titration rate of a) and d) 0.5 mL/min; b) and e) 20 mL/min: c) and f) maximum titration rate (about 600 mL/min for small volume, about 800 mL/min for large volume). Scale bar is 2 μm. The values on the pictures correspond to the titration rate reported to the volume.

Fig. 10. a) Effect of the addition rate relative to total volume on the size dispersion measured by SEM images analysis; b) particle size distribution obtained by laser diffraction in function of addition rate. Narrowing (decrease of size dispersion) and displacement to higher values with increase of addition rate are obvious.

4.2. Productivity

One of the problems related to the production method used here, is the very low productivity of the reaction. Indeed, only 0.3–0.4 g/L CaP particles (β-TCP and/or DCP) were produced in the best conditions. Concerning β-TCP, obtained at high pH, an attempt was made to increase the concentrations, but the solubility of the phosphate precursor is limited to about 1.33 M in ethylene glycol. Furthermore, a concentration increase at high pH led to a change of precipitated phase: whereas β-TCP was the main phase obtained in standard conditions (16 mM), only a mixture of DCP and apatite was obtained at 64 mM (Figs. 11 and 12). Since DCP is a more acidic phase than β-TCP, it was supposed that the use of a higher pH might hinder DCP precipitation and favour β-TCP. Unfortunately, an increase of the pH at pH10 impaired the precipitation (see supporting information, Fig. S4). Nevertheless, it was possible to increase the reaction volume from 70 to 500 mL without significant changes in particle size, size dispersion and agglomeration (Fig. 5). In other words, upscaling the precipitation synthesis seems to be feasible. It is surprising that the yield is only 30% at 16 mM, even though precipitates were still observed at 1.6 mM. If precipitation is observed for a solution of 1.6 mM, a 10-fold increase of the concentration would be expected to result in a yield much higher than 30%. This suggests that the solubility of β-TCP is very low in ethylene glycol, but that a lot of precipitates must be lost during processing, for example during centrifugation. For comparison, large batches at 150 °C and low pH (pH 4) also yielded 0.3–0.4 g/L of DCP platelets. However the precursors' concentration could easily be doubled without occurrence of another crystalline phase and the productivity was increased to 0.8–0.9 g/L without influence on crystal size and composition (results not shown).

4.3. CaP crystal shape

Since the CaP platelet synthesis was reproducible and feasible in reasonable amounts, the next important requirement was first to relate crystal shape and composition, and then explain the crystal habit based on the crystalline structure. SEM observations (Figs. 8 and 13) suggest that the DCP crystals identified by XRD always crystallized in the form of parallelepipeds, whereas the β-TCP
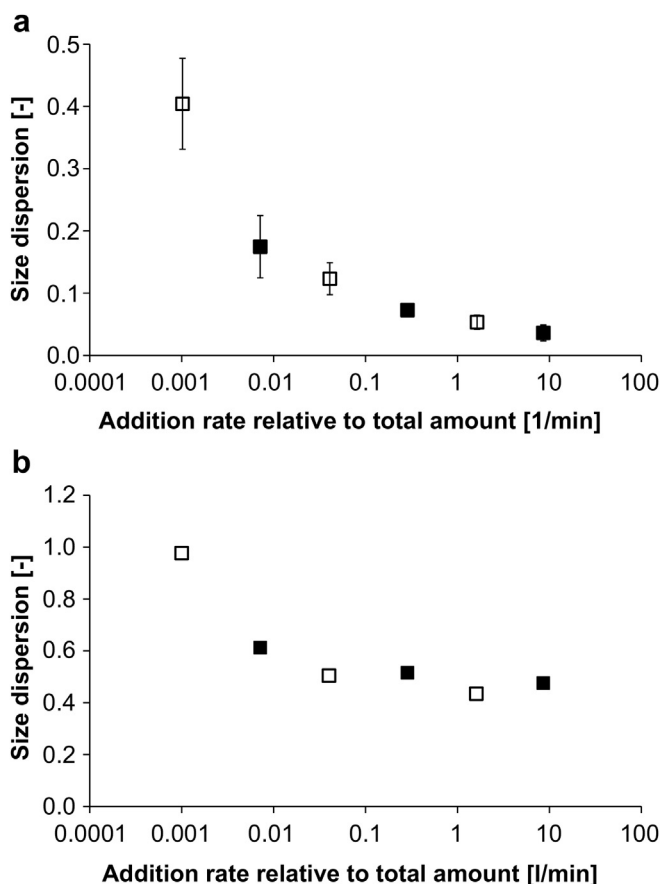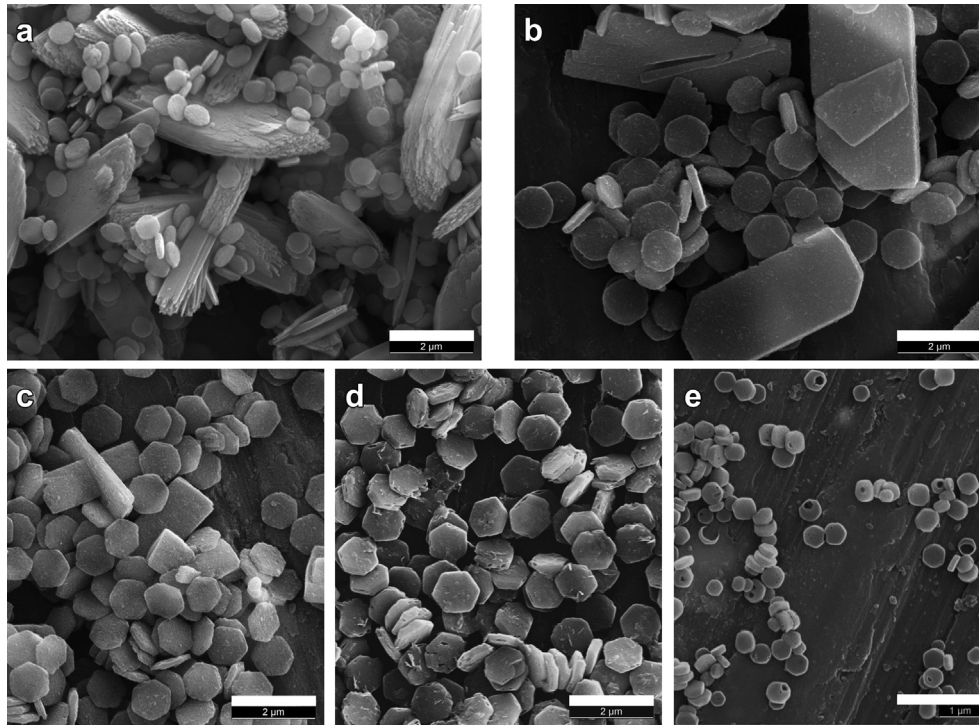
Fig. 11. Representative SEM pictures of samples synthesized at a) 90 °C; b) 110 °C; c) 130 °C; d) 150 °C; e) 170 °C.

crystals precipitated as almost regular octahedrons or hexagonal prisms. Regarding the crystal habit, DCP crystallizes in the triclinic crystal system and is known to adopt a parallelepiped shape [40] as observed here. The crystal habits of β-TCP crystals are more surprising. The lattice system of β-TCP is rhombohedral which belongs to the trigonal crystal system and the hexagonal crystal family. The most common crystal form of whitlockite — the naturally occurring phase isostructural to β-TCP — is represented in Fig. 18a. The [001] planes can become regular hexagons (Fig. 18b) if the side faces (e.g. [104] and [102] planes) grow at similar rates. Similarly, platelets are formed when the [001] planes (identified by preferred orientation in XRD) have the slowest growth rate. Hexagonal prisms crystalline habits are thus not surprising. No SAED patterns were measured in the present study, hence the side planes were not identified. Tao et al. stated that the side faces of the hexagons were perpendicular
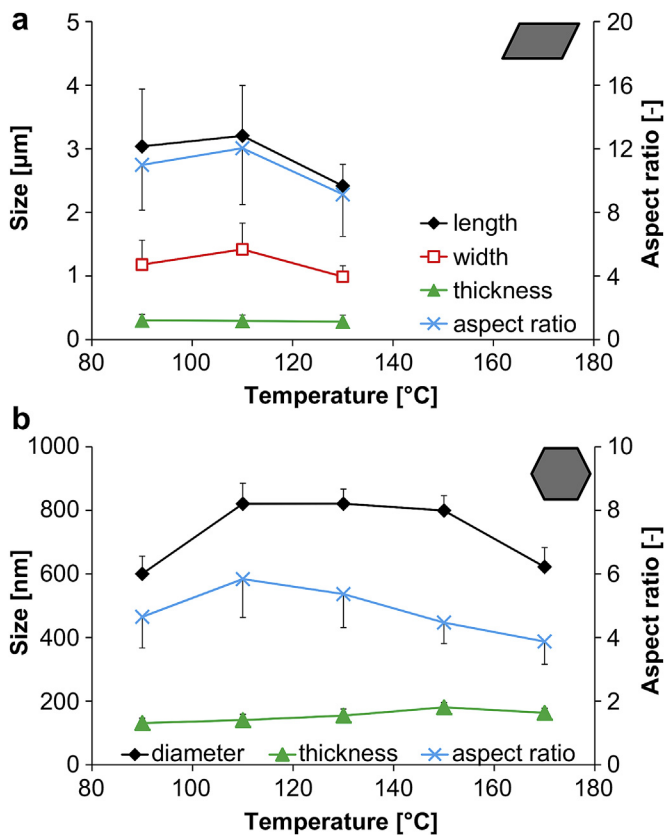

Fig. 12. Effect of the reaction temperature on the dimensions of a) parallelepiped crystals and b) hexagonal β-TCP platelets measured on SEM images. Left axis: length, diameter and thickness. Right axis: aspect ratio.
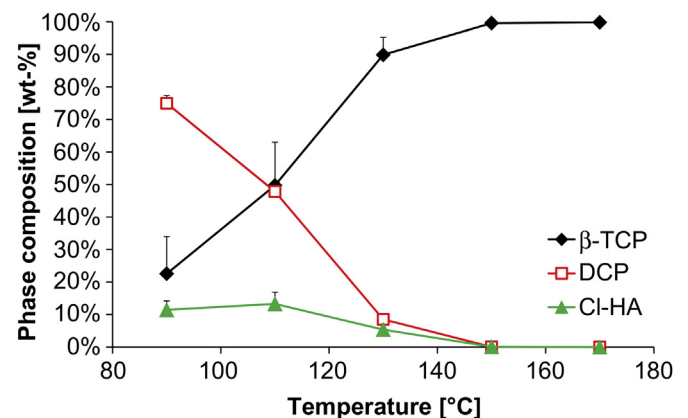

Fig. 13. Effect of the synthesis temperature on the crystalline phase (obtained from Rietveld refinement of XRD measurements).
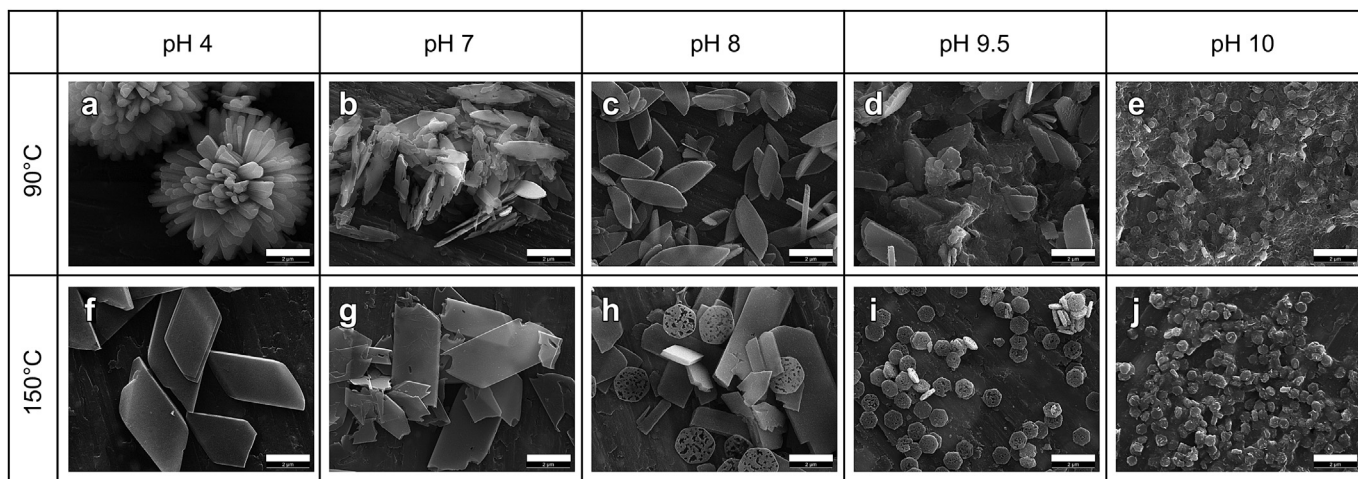
Fig. 14. SEM images of particles obtained at 90 °C (a–e) or 150 °C (f–j), and pH 4 (a + f), pH 7 (b + g), pH 8 (c + h), pH 9.5 (d + i) or pH 10 (e + j). Scale bar is 2 µm on all images.

to the [001] planes [35], but considering the rounded edges observed in the present study on SEM images and the crystal habit of whitlockite, the planes of the crystal side faces might be other family planes.

The formation of regular octahedrons is more surprising in a trigonal crystal system. It is assumed that the crystals are pseudo-octahedrons and that they are formed when the [001] planes and some of the side planes grow slowly at equal growth rates (Fig. 18c).

The indices of those planes were not investigated here. Tao et al. proposed [111], [101] or [001] planes. However, these authors did not obtain β-TCP octahedrons by changing the precursor concentration but by using other precursors.

In the present study, there is a slow transition from a globular/compact shape at low concentration (pseudo-regular octahedrons) to a planar shape at high concentration (hexagonal prisms; Fig. 6). At intermediate concentration (8 mM), transitional shapes between
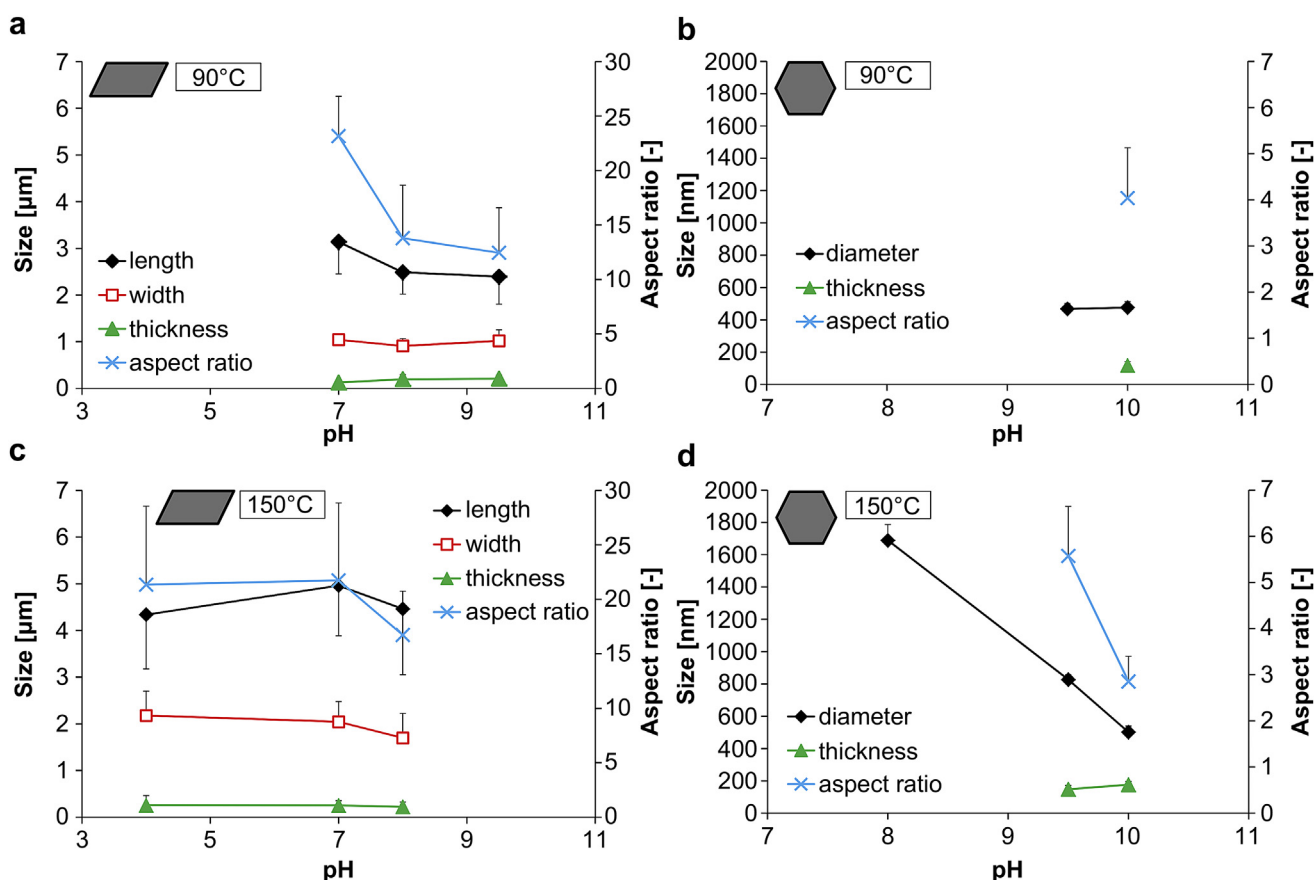

Fig. 15. Effect of the pH on the dimensions of a) and c) parallelepiped crystals and b) and d) hexagonal crystals at a) and b) 90 °C and c) and d) 150 °C: diameter or length (diamonds, left axis), width (squares, left axis), thickness (triangles, left axis) and aspect ratio (cross, right axis).
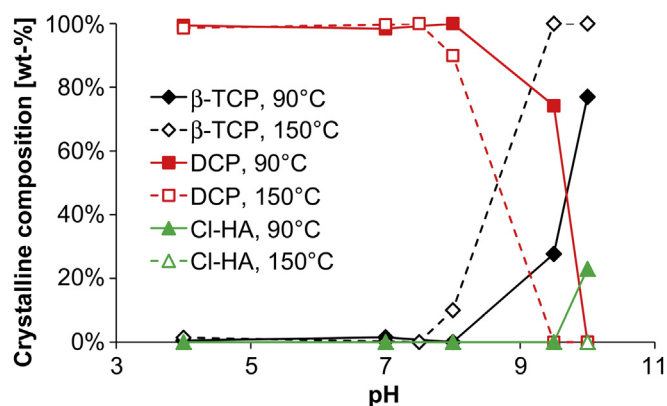
Fig. 16. Effect of the pH on the crystalline phase: at low pH, monetite is formed. β-TCP then appears, at lower pH at 150 °C (dashed lines) than at 90 °C (continuous lines). Hence 100% β-TCP is reached with a pH of 9.5 at 150 °C whereas a slightly higher pH (10) is required at 90 °C to avoid DCP.

Table 2
Dimensions of the platelets obtained with different volumes and titration rates ($n = 1$). The titration rate can be expressed either as volume of solution per unit of time (mL/min) or relatively to the total volume (min^{-1}).

Volume [mL]	Titration rate [mL/min]	[min^{-1}]	n	Diameter [nm]	Size dispersion	Thickness [nm]	Aspect ratio
70	0.5	0.007	1	447 ± 95	0.21	135 ± 30	3.3 ± 1.4
70	20	0.3	1	527 ± 38	0.07	147 ± 15	3.6 ± 0.6
70	600	9	5	853 ± 33	0.04 ± 0.01	164 ± 18	5.0 ± 0.7
500	0.5	0.001	1	415 ± 178	0.43	415 ± 178	1.0 ± 0.9
500	20	0.04	1	501 ± 53	0.11	128 ± 16	3.9 ± 0.9
500	800	1.6	6	844 ± 45	0.05 ± 0.01	151 ± 19	5.6 ± 1.0

hexagonal prism and regular octahedron were observed. Some other examples of intermediate shapes are also shown in the supplementary data (Figs. S7, S8). This concentration dependence of the crystal shape is typical for precipitation reactions [41]. At low concentrations the shape is dominated by nucleation requirements (nearly spherical but still faceted shapes, minimizing the surface per volume). According to Ref. [42], an increase of the supersaturation favours the growth of specific crystal faces, leading to more elongated crystals.

Tao et al. explained the precipitation of β-TCP in the form of hexagonal prisms in the solution $CaCl_2-Na_2HPO_4-EG$ by surface energy calculations [35]. They showed that the octahedron formation in $CaCl_2-Na_2HPO_4-EG$ solution is thermodynamically unfavourable for its relatively large interfacial energy, but the smallest specific surface of the octahedral crystals is apparently favoured at lower concentrations. However, these authors did not make calculations using different precursor concentrations.

For both phases, the particles became more angular and adopted a more idiomorphic crystal form with increasing temperature (Fig. 11), similar to the observation of Tao et al. for β-TCP [35]. However, the particles size and shape did not change when the reaction time was increased from 1.5 h to 24 h, suggesting that the
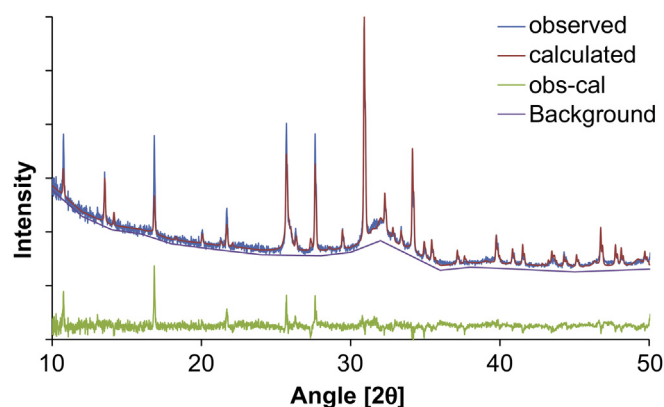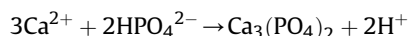

Fig. 17. XRD diagram of the sample precipitated at 90 °C pH 10. The observed diffraction diagram (blue line) was fitted with a calculated model (red line). The large differences (green line, "obs−cal") at peak positions are due to a strong crystalline orientation. The β-TCP and chloroapatite peaks were identified and refined with Rietveld analysis. The broad peaks and the high background (purple line) indicate the presence of an amorphous phase. (For interpretation of the references to colour in this figure legend, the reader is referred to the web version of this article.)

hexagonal and parallelepiped shapes were already the least energetic configuration for β-TCP and DCP crystals, respectively (see supplementary data Fig. S1).

4.4. Crystal purity

Four different CaP phases were obtained in all precipitation experiments performed in this study: DCP, β-TCP, chloroapatite, and an amorphous phase. From these four CaP phases, DCP and β-TCP constituted almost 100% of all precipitates retrieved in the various experiments (Figs. 4, 8, 13 and 17). Except for a few exceptions, as at high concentrations, the other phases only occurred in trace amounts.

Contrary to β-TCP, DCP formation was favoured at a low pH value (Fig. 16), low temperature (Fig. 13) and a high concentration (Fig. 8). The predominance of DCP at low pH values is logical considering the respective solubilities of DCP and β-TCP phases. For example, Vereecke and Lemaître [43] calculated that in the system $Ca(OH)_2-H_3PO_4-KOH-HNO_3-CO_2-H_2O$, DCP was more stable than β-TCP below a pH value of 6.3−6.4. Interestingly, their data also showed that the pH stability range of β-TCP (compared to DCP) enlarged with an increase of temperature. Assuming that this type of behaviour can be extrapolated to ethylene glycol, β-TCP formation should not only be favoured at high pH but also at high temperature, which was observed in our study. However, it is questionable to extrapolate data from an aqueous to a non-aqueous system. Indeed, whereas three CaP phases precipitate in physiological conditions (DCP at low pH (<6), OCP at intermediate pH ($\sim 6-7$)) and HA in basic conditions, usually only two main phases formed in ethylene glycol: DCP and β-TCP. Furthermore, one of these two phases, β-TCP, has never been reported to form in aqueous conditions. Tao et al. proposed that ethylene glycol slowly released calcium and phosphate ions, hence maintaining a low but stable driving force during precipitation [34]. This promoted the formation of the well-crystallized β-TCP crystals which normally do not appear in aqueous solution. Indeed it is known that the divalent calcium ions can be chelated by ethylene glycol [44,45]. In addition to low pH and temperature, an increase in precursor concentration also favoured DCP formation. This can be expected looking at the chemical reaction:

$$3Ca^{2+} + 2HPO_4{}^{2-} \rightarrow Ca_3(PO_4)_2 + 2H^+$$

During β-TCP formation, hydronium ions are released leading to an acidification of the solution. Therefore, the higher the precursor concentration is, the more H$^+$ are released, favouring the acidic monetite phase.

Besides DCP and β-TCP, chloroapatite was also observed (e.g. 90 °C, pH 10), but the amounts usually remained low (Figs. 13 and 16). The formation of an apatite compound is expected, especially at high pH, considering that HA is the most stable CaP phase in neutral
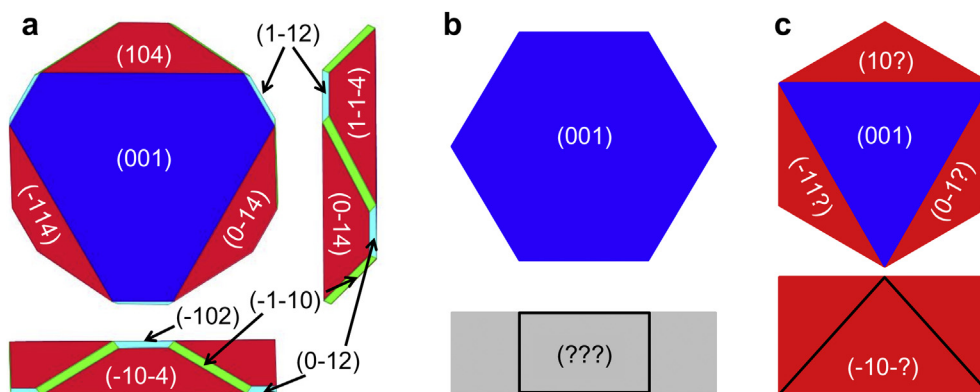
Fig. 18. a) Trigonal crystal habit of the whitlockite (webmineral.com) from the top and the sides. Indice of dark blue faces is (001), of red is (104), of cyan is (102) and of green is (110). b) Hexagonal prisms derived from the trigonal crystal habit in a, top and side view. c) Regular hexagon derived from the trigonal crystal habit in a, top and side view. (For interpretation of the references to colour in this figure legend, the reader is referred to the web version of this article.)

and basic aqueous solutions [43]. Furthermore, Weng et al. [46] and Gopi et al. [47] have reported the precipitation of apatite in ethylene glycol using other precursors but obtained agglomerated particles with irregular or globular morphology.

The last phase that was observed was amorphous calcium phosphate. The occurrence of an amorphous precursor at the beginning of a biomineralization process is not surprising [48]. Its presence in some samples thus indicates an incomplete crystallization.

Hence, only two crystal phases were produced pure: β-TCP and DCP. Since DCP and β-TCP platelets have very different morphologies, it is essential to either produce pure β-TCP or pure DCP. Indeed, a mixture of these two phases would lead to a bi-modal size distribution and therewith to a less ideal composite structure. Currently, it is difficult to say which phase would be the most efficient to reinforce a composite. Regarding the mechanical properties, *ab initio* calculations were published for β-TCP [49], but not for monetite. However, considering the higher thermodynamical stability of β-TCP compared to that of DCP (lower solubility, higher melting point), β-TCP is expected to be stronger than DCP. Nevertheless, not only the tensile strength but also the aspect ratio affects the mechanical properties of the composite [19].

4.5. Aspect ratio

In general, the DCP parallelepiped platelets presented higher aspect ratios than β-TCP platelets. The values for DCP platelets varied between 8 and 25, whereas the highest aspect ratio obtained with β-TCP platelets was 10 (Fig. 7). Pure β-TCP platelets, on the other hand, were only obtained with an aspect ratio of max. 6. In comparison, Tao et al. [35] did not obtain DCP platelets and did not report aspect ratios superior to 4 for β-TCP.

The aspect ratio could be influenced by different reaction parameters such as titration rate (for β-TCP), temperature (for both phases), concentration (for β-TCP) and pH value (for both phases). The most effective parameters were the concentration and the pH value. For example, β-TCP aspect ratio increased from 1 to 10 with a concentration increase from 1.6 to 32 mM (Fig. 7). Similarly, DCP aspect ratio increased from 12 to 25 when the pH value was reduced from 9.5 to 7.0 (Fig. 15a). As previously explained, the effect of concentration on the β-TCP aspect ratio (Fig. 7) is related to the general trend that platelets grow wider and thinner with increasing supersaturation [41]. The effect seen for pH alterations might be due to modifications of crystal surface charges [41] or to supersaturation changes with pH [50]. An increase of the temperature also slightly reduced the aspect ratio of the crystals

(Fig. 12). This suggests that the solubility increased with the temperature, which increased the nucleation rate but limited crystal growth [50]. Indeed, a rise of solubility reduces the supersaturation and in consequence the differences in growth rates between side and surface faces decreased and with it the aspect ratio decreased [41].

Ideally, a large aspect ratio is required to efficiently reinforce a polymer–ceramic composite as it allows an adequate stress transfer between the polymer matrix and the ceramic reinforcement [19]. Based on the present results, the DCP platelets produced with an aspect ratio of 25 appear to be the most interesting.

4.6. Critical thickness

Ceramic materials break in a brittle manner by catastrophic crack propagation. Pre-existing defects, particularly large ones, act like a stress concentrator. As a result, the experimental strength hardly reaches the theoretical strength of the material. For example, dense polycrystalline β-TCP reaches a tensile strength of 154 MPa [51], whereas its theoretical strength lies between 1 and 10 GPa, i.e. 1–10% of the theoretical Young's modulus value of 110 GPa [49]. When the size of the ceramic parts is reduced, the size of the largest defects is also reduced. Consequently, rupture happens at higher stresses. Whereas when the largest defects become smaller than a critical value (Griffith criterion) [20], they are not able to concentrate stresses and the theoretical rupture strength is reached. In case of β-TCP, the critical thickness was estimated to be close to 350 nm, based on theoretical mechanical properties [49] (Suppl. data). An estimation for DCP was not possible, because no *ab initio* calculated mechanical properties could be found in the literature. However, as previously mentioned DCP Young's modulus is certainly similar or smaller than the β-TCP modulus. Since the weaker a ceramic is, the larger is its critical thickness [19], the critical thickness of DCP is certainly close to or above the one of β-TCP, i.e. ≥350 nm. In the present study, both types of obtained platelets were thinner than 300 nm, i.e. thin enough to reach the theoretical strength.

The optimum thickness and aspect ratio of ceramic reinforcement are pre-requisite to achieve an efficient reinforcement of a ductile matrix, but not only. In addition it is necessary that the reinforcement particles have homogeneous properties, otherwise local variations may weaken the structure. For example, particles from a weaker phase might break first leading to local catastrophic failure. Therefore, the size dispersion of the primary particles should be as narrow as possible and they should not be agglomerated.

4.7. Uniformity of primary particles

In the present study, the size dispersion was generally below 0.10 for β-TCP particles, and between 0.20 and 0.30 for parallelepiped platelets (Figs. 3, 7, 10, 12 and 15). As monodispersity is generally defined as <0.10 [52], only β-TCP crystals can be considered to be monodisperse. Such a narrow particle size distribution is typical for diffusion-controlled reactions [33,53] and often seen for the synthesis of oxides in organic media [54,55]. A comparison with the literature is difficult because particle size distribution measurements are rarely performed − or mentioned − for CaP powders, perhaps because the size distribution is too broad and/or the particles often are strongly agglomerated. For example, the lowest size dispersion that could be estimated on SEM pictures from the literature was 0.2−0.3 [27,28].

The precipitation of very uniform particles can be explained by a combination of the LaMer model [56,57] and a diffusion-controlled growth. In the LaMer model, nucleation is so rapid that a high supersaturation, occurring for example after quickly adding the phosphate solution into the calcium solution, is only transitory (Fig. 19, adapted from Refs. [33,56]). In other words, all nuclei form simultaneously, resulting in a rapid drop of the concentration, therewith impairing further nucleation. The subsequent growth history is then identical for all nuclei.

On the other hand, when titration is slow, nucleation occurs during the whole titration period, hence leading to various growth histories (Fig. 19), i.e. various particle sizes. The LaMer-type nucleation is not the only pre-requisite to obtain a narrow size distribution. It is also necessary to have a diffusion-controlled growth for which the concentration gradient (and hence the growth rate) is inversely proportional to the particle radius. In other words, small particles grow faster than large particles [42], thus preventing coarsening or ripening [58] and resulting in a narrowing of the PSD. According to the theory, this effect is particularly strong at high concentrations but the present results demonstrate that uniform particles can be obtained at low concentrations (Fig. 7). An additional experiment further confirmed that the growth of the present system is diffusion-controlled. By lowering the stirring rate, the particle size distribution increased (Fig. S6). This is typical for diffusion-controlled processes [50].

Interestingly, the narrow size distribution of β-TCP crystals obtained at high titration rate remained stable over time, suggesting that Ostwald ripening (dissolution of the smallest particles to feed the growth of the largest ones) was negligible [33] (Fig. S1).

The DCP size dispersion is slightly larger than that of β-TCP, suggesting that the nucleation and/or growth mechanisms are not fully identical, but currently only speculations can be made about this difference. To get more insights, growth kinetics studies should be performed, but these will be done in a subsequent stage.

4.8. Non-agglomerated

Last, but not least, to ensure optimal performances of a composite material, agglomeration of the reinforcement particles should be minimal. Luckily, most particles appeared to be fairly well dispersed. This was expressed by the narrow monomodal size dispersion measured by laser diffraction. However, one parameter seemed to negatively affect the degree of agglomeration. A slow titration rate of the phosphate precursor tended to promote the formation of agglomerates [59], as observed on SEM images (Fig. 9a, b, d), which could however be separated by ultrasonication (as observed by laser diffraction measurements). Since nuclei are formed during the entire titration period, it is assumed that at slow titration rates, pre-existing particles served as seeds for new particles, hence forming agglomerates [59]. Moreover, phosphate ions are known to act as dispersant. Hence adding them slowly increases agglomeration. In other words, high titration rates ensured a low degree of agglomeration.

The platelets were not more agglomerated after 24 h than after 1.5 h, demonstrating the efficiency of ethylene glycol to disperse and stabilize β-TCP particles and thus maintaining a constant particle size and shape over time (Fig. S1). This stabilizing effect is attributed to the formation of chelates between the OH groups of the ethylene glycol molecules and calcium ions [60].

4.9. General points

The aim of this study was to synthesize reproducible CaP particles of controlled thickness, aspect ratio and composition, with a low degree of agglomeration and high productivity. The results show that it is indeed possible to achieve most requirements. However, pure β-TCP platelets could not be produced with an aspect ratio larger than 6 and DCP platelets tended to be agglomerated and presented a non-uniform particle size distribution. In a ceramic-reinforced polymer composite, a low aspect ratio and a high degree of agglomeration of ceramic particles are expected to be detrimental to the tensile properties. Therefore, based on the present study, a choice has to be made between β-TCP particles with high uniformity and low aspect ratios and monetite particles with low uniformity but high aspect ratios. Such a choice may not only affect the mechanical properties of the composite, but also its biological properties. β-TCP is indeed less soluble than DCP in physiological conditions and hence is expected to resorb slower [6]. However, to our knowledge, there is no *in vivo* study demonstrating a difference between these two materials.

The present study shows that β-TCP platelets with aspect ratio >6 can be obtained at pH 8 and at a high concentration but with concomitant formation of DCP. Since the pH was only controlled at the start of the reaction, it might be of interest to monitor and control the pH value during the reaction.

One of the problems raised by the present study is the difficulty to increase the productivity. The solubility of the raw materials is very low, hence limiting the productivity to 0.3−0.4 g/L. Even though the volume can be increased, uniform particles can only be obtained at high titration rates (Fig. 10), which is likely to be a problem for much bigger batches. Tubular reactors may be considered. These types of reactors are particularly interesting for reactions finished within a few minutes, as suggested by Tao et al. [35].
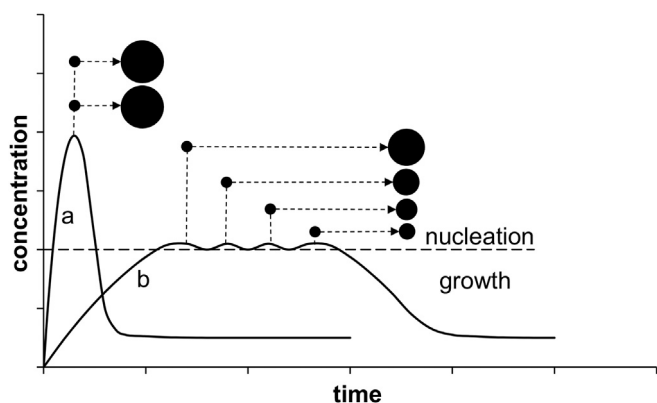

Fig. 19. Nucleation and growth mechanism with a) fast and b) slow concentration increase leading to narrow and broad particle size distribution, respectively (adapted from Ref. [33,56]).

5. Conclusions

Precipitating CaP particles in ethylene glycol is a very effective method to obtain non-agglomerated CaP particles with well-defined composition, size and shape. In the best conditions, the particle size dispersion sank below 5% for β-TCP and below 20% for DCP. The size and shape were tuneable by means of precursors' concentration, pH and temperature. Samples of pure uniform hexagonal β-TCP platelets were obtained at high pH and high temperature. The diameter and aspect ratio ranged from 170 to 870 nm and from 1 to 5, respectively. When mixed with DCP, aspect ratios superior to 10 were obtained. Pure monetite platelets were obtained in acidic and neutral pH conditions, with some variations in particle shape and size according to the temperature and pH. The particles showing the largest aspect ratio (close to 25) were monetite parallelepiped platelets obtained at 90 °C and at pH 7. However, these particles had a broader size dispersion than β-TCP hexagonal platelets and appeared more agglomerated. The ideal platelets are a trade-off between a large aspect ratio, a pure composition, uniformity (monodispersity), sub-micrometric dimensions and a low degree of agglomeration but these properties are controllable by mean of reaction temperature, pH, titration rate and precursors' concentration.

Appendix A. Supplementary data

Supplementary data related to this article can be found at http://dx.doi.org/10.1016/j.biomaterials.2013.05.026.

References

[1] Laurencin C, Khan Y, El-Amin SF. Bone graft substitutes. Expert Rev Med Devices 2006;3(1):49—57.
[2] Banwart JC, Asher MA, Hassanein RS. Iliac crest bone graft harvest donor site morbidity. A statistical evaluation. Spine 1995;20(9):1055—60.
[3] Younger EM, Chapman MW. Morbidity at bone graft donor sites. J Orthop Trauma 1989;3(3):192—5.
[4] LeGeros RZ. Properties of osteoconductive biomaterials: calcium phosphates. Clin Orthop 2002;(395):81—98.
[5] Bohner M. Resorbable biomaterials as bone graft substitutes. Mater Today 2010;13(1—2):24—30.
[6] Bohner M. Calcium orthophosphates in medicine: from ceramics to calcium phosphate cements. Injury 2000;31(Suppl. 4):37—47.
[7] Eggli PS, Muller W, Schenk RK. Porous hydroxyapatite and tricalcium phosphate cylinders with two different pore size ranges implanted in the cancellous bone of rabbits. A comparative histomorphometric and histologic study of bony ingrowth and implant substitution. Clin Orthop 1988;(232):127—38.
[8] Kanatani M, Sugimoto T, Fukase M, Fujita T. Effect of elevated extracellular calcium on the proliferation of osteoblastic MC3T3-E1 cells: its direct and indirect effects via monocytes. Biochem Biophys Res Commun 1991;181(3):1425—30.
[9] Bohner M, Theiss F, Apelt D, Hirsiger W, Houriet R, Rizzoli G, et al. Compositional changes of a dicalcium phosphate dihydrate cement after implantation in sheep. Biomaterials 2003;24(20):3463—74.
[10] Tamimi F, Torres J, Gbureck U, Lopez-Cabarcos E, Bassett DC, Alkhraisat MH, et al. Craniofacial vertical bone augmentation: a comparison between 3D printed monolithic monetite blocks and autologous onlay grafts in the rabbit. Biomaterials 2009;30(31):6318—26.
[11] Tamimi F, Nihouannen DL, Eimar H, Sheikh Z, Komarova S, Barralet J. The effect of autoclaving on the physical and biological properties of dicalcium phosphate dihydrate bioceramics: brushite vs. monetite. Acta Biomater 2012;8(8):3161—9.
[12] Wagoner Johnson AJ, Herschler BA. A review of the mechanical behavior of CaP and CaP/polymer composites for applications in bone replacement and repair. Acta Biomater 2011;7(1):16—30.
[13] Rezwan K, Chen QZ, Blaker JJ, Boccaccini AR. Biodegradable and bioactive porous polymer/inorganic composite scaffolds for bone tissue engineering. Biomaterials 2006;27(18):3413—31.
[14] Bonderer LJ, Studart AR, Gauckler LJ. Bioinspired design and assembly of platelet reinforced polymer films. Science 2008;319(5866):1069—73.
[15] Podsiadlo P, Kaushik AK, Arruda EM, Waas AM, Shim BS, Xu J, et al. Ultrastrong and stiff layered polymer nanocomposites. Science 2007;318(5847):80—3.
[16] Thornton C, Yin KK, Adams MJ. Numerical simulation of the impact fracture and fragmentation of agglomerates. J Phys D Appl Phys 1996;29(2):424—35.
[17] Zhang Y, Evans JRG. Approaches to the manufacture of layered nanocomposites. Appl Surf Sci 2012;258(6):2098—102.
[18] Rexer J, Anderson E. Composites with planar reinforcements (flakes, ribbons) — a review. Polym Eng Sci 1979;19(1):1—11.
[19] Gao H. Application of fracture mechanics concepts to hierarchical biomechanics of bone and bone-like materials. Int J Fract 2006;138(1—4):101—37.
[20] Griffith AA. The phenomena of rupture and flow in solids. Philos Trans R Soc Lond 1921;221:163—98.
[21] Ji B, Gao H. Mechanical properties of nanostructure of biological materials. J Mech Phys Solids 2004;52:1963—90.
[22] LeGeros RZ, LeGeros JP. Calcium phosphate bioceramics: past, present and future. Key Eng Mat 2003;240-2:3—10.
[23] Gibson IR, Ke S, Best SM, Bonfield W. Effect of powder characteristics on the sinterability of hydroxyapatite powders. J Mater Sci Mater Med 2001;12(2):163—71.
[24] Layrolle P, Lebugle A. Characterization and reactivity of nanosized calcium phosphates prepared in anhydrous ethanol. Chem Mater 1994;6(11):1996—2004.
[25] Layrolle P, Lebugle A. Synthesis in pure ethanol and characterization of nanosized calcium phosphate fluoroapatite. Chem Mater 1996;8(1):134—44.
[26] Wang P, Li C, Gong H, Jiang X, Wang H, Li K. Effects of synthesis conditions on the morphology of hydroxyapatite nanoparticles produced by wet chemical process. Powder Technol 2010;203(2):315—21.
[27] Zhang H, Darvell BW. Synthesis and characterization of hydroxyapatite whiskers by hydrothermal homogeneous precipitation using acetamide. Acta Biomater 2010;6(8):3216—22.
[28] Zhang H, Darvell BW. Constitution and morphology of hydroxyapatite whiskers prepared using amine additives. J Eur Ceram Soc 2010;30(10):2041—8.
[29] Neira IS, Guitian F, Taniguchi T, Watanabe T, Yoshimura M. Hydrothermal synthesis of hydroxyapatite whiskers with sharp faceted hexagonal morphology. J Mater Sci 2008;43(7):2171—8.
[30] Neira IS, Kolen'ko YV, Lebedev OI, Van Tendeloo G, Gupta HS, Guitian F, et al. An effective morphology control of hydroxyapatite crystals via hydrothermal synthesis. Cryst Growth Des 2009;9(1):466—74.
[31] Jinawath S, Pongkao D, Suchanek W, Yoshimura M. Hydrothermal synthesis of monetite and hydroxyapatite from monocalcium phosphate monohydrate. Int J Inorg Mater 2001;3(7):997—1001.
[32] Zhang Hb, Zhou Kc, Li Zy, Huang Sp. Plate-like hydroxyapatite nanoparticles synthesized by the hydrothermal method. J Phys Chem Solids 2009;70(1):243—8.
[33] Kwon SG, Hyeon T. Formation mechanisms of uniform nanocrystals via hot-injection and heat-up methods. Small 2011;7(19):2685—702.
[34] Tao J, Jiang W, Zhai H, Pan H, Xu R, Tang R. Structural components and anisotropic dissolution behaviors in one hexagonal single crystal of β-tricalcium phosphate. Cryst Growth Des 2008;8(7):2227—34.
[35] Tao J, Pan H, Zhai H, Wang J, Li L, Wu J, et al. Controls of tricalcium phosphate single-crystal formation from its amorphous precursor by interfacial energy. Cryst Growth Des 2009;9(7):3154—60.
[36] Rodriguez-Carvajal J. Recent developments of the program FULLPROF, vol. 26. Commission on Powder Diffraction (IUCr) Newsletter; 2001. p. 12—9. Epub 3.40.
[37] Dickens B, Schroeder LW, Brown WE. Crystallographic studies on the role of Mg as a stabilizing impurity in β-Ca₃(PO₄)₂. I. The crystal structure of pure β-Ca₃(PO₄)₂. J Solid State Chem 1974;10:232—48.
[38] Dickens B, Bowen JS, Brown WE. A refinement of the crystal structure of CaHPO₄ (synthetic monetite). Acta Crystallogr 1971;B28:797—806.
[39] Sudarsanan K, Young RA. Significant precision in crystal structure details: Holly springs hydroxyapatite. Acta Crystallogr 1969;B25:1534—43.
[40] Chenot CF, Inventor, GTE Sylvania Incorporated, Assignee. Method of converting brushite to monetite crystals with controlled variation in crystal habit. USA patent US Patent 3927180; 1975.
[41] Boistelle R, Astier JP. Crystallization mechanisms in solution. J Cryst Growth 1988;90(1—3):14—30.
[42] Peng X, Manna L, Yang W, Wickham J, Scher E, Kadavanich A, et al. Shape control of CdSe nanocrystals. Nature 2000;404(6773):59—61.
[43] Vereecke G, Lemaître J. Calculation of the solubility diagrams in the system Ca(OH)₂-H₃PO₄-KOH-HNO₃-CO₂-H₂O. J Cryst Growth 1990;104:820—32.
[44] Zhang X, Liu J, Yu H, Yang G, Wang J, Yu Z, et al. Enhanced electrochemical performances of LiNi₀.₅Mn₁.₅O₄ spinel via ethylene glycol-assisted synthesis. Electrochim Acta 2010;55(7):2414—7.
[45] Knetsch D, Groeneveld WL. Alcohol as ligands. III. Complexes of ethylene glycol with some divalent metal halides. Inorg Chim Acta 1973;7(C):81—7.
[46] Weng W, Baptista JL. A new synthesis of hydroxyapatite. J Eur Ceram Soc 1997;17(9):1151—6.
[47] Gopi D, Bhalaji PR, Prakash VCA, Ramasamy AK, Kavitha L, Ferreira JMF. An effective and facile synthesis of hydroxyapatite powders using oxalic acid-ethylene glycol mixture. Curr Appl Phys 2011;11(3):590—3.
[48] Addadi L, Vidavsky N, Weiner S. Transient precursor amorphous phases in biomineralization. In the footsteps of Heinz A. Lowenstam. Z Kristallogr 2012;227(11):711—7.
[49] Liang L, Rulis P, Ching WY. Mechanical properties, electronic structure and bonding of α-and β-tricalcium phosphates with surface characterization. Acta Biomater 2010;6(9):3763—71.
[50] Rodríguez-Hornedo N, Murphy D. Significance of controlling crystallization mechanisms and kinetics in pharmaceutical systems. J Pharm Sci 1999;88(7):651—60.
[51] Jarcho M, Salsbury RL, Thomas MB, Doremus RH. Synthesis and fabrication of b-tricalcium phosphate (whitlockite) ceramics for potential prosthetic applications. J Mater Sci 1979;14:142—50.

[52] Inukai S, Tanma T, Orihara S, Konno M. A simple method for producing micron-sized, highly monodisperse polystyrene particles in aqueous media: effects of impeller speed on particle size distribution. Chem Eng Res Des 2001;79(8):901–5.

[53] Murray CB, Norris DJ, Bawendi MG. Synthesis and characterization of nearly monodisperse CdE (E = S, Se, Te) semiconductor nanocrystallites. J Am Chem Soc 1993;115(19):8706–15.

[54] Feldmann C. Polyol-mediated synthesis of nanoscale functional materials. Adv Funct Mater 2003;13(2):101–7.

[55] Jana NR, Chen Y, Peng X. Size- and shape-controlled magnetic (Cr, Mn, Fe, Co, Ni) oxide nanocrystals via a simple and general approach. Chem Mater 2004;16(20):3931–5.

[56] Tao AR, Habas S, Yang P. Shape control of colloidal metal nanocrystals. Small 2008;4(3):310–25.

[57] Lamer VK, Dinegar RH. Theory, production and mechanism of formation of monodispersed hydrosols. J Am Chem Soc 1950;72(11):4847–54.

[58] Barnard AS. Modelling of nanoparticles: approaches to morphology and evolution. Rep Prog Phys 2010;73(8).

[59] Nichols G, Byard S, Bloxham MJ, Botterill J, Dawson NJ, Dennis A, et al. A review of the terms agglomerate and aggregate with a recommendation for nomenclature used in powder and particle characterization. J Pharm Sci 2002;91(10):2103–9.

[60] Wilkinson A, McNaught AD. IUPAC. Compendium of chemical terminology (the "gold book"). 2.3.1 ed. Oxford: Blackwell Scientific Publications; 1997.